Biophysical Journal Volume 96 February 2009 951–963

Predictions Suggesting a Participation of β-Sheet Configuration in the M2 Domain of the $P2X_7$ Receptor: A Novel Conformation?

Pedro Celso Nogueira Teixeira,[†] Cristina Alves Magalhães de Souza,[‡] Mônica Santos de Freitas,[§] Débora Foguel,[§] Ernesto Raul Caffarena,[¶] and Luiz Anastacio Alves[‡*]

[†]Fundação Mokiti Okada, Centro de Pesquisa; [‡]Fundação Oswaldo Cruz, Laboratório de Comunicação Celular, Instituto Oswaldo Cruz; [§]Programa de Biologia Estrutural, Instituto de Bioquímica Médica, Centro Nacional de Ressonância Magnética Nuclear Jiri Jonas, Universidade Federal do Rio de Janeiro; and [¶]Fundação Oswaldo Cruz, Programa Computação Científica, Rio de Janeiro, Brazil

ABSTRACT Scanning experiments have shown that the putative TM2 domain of the $P2X_7$ receptor ($P2X_7R$) lines the ionic pore. However, none has identified an α-helix structure, the paradigmatic secondary structure of ion channels in mammalian cells. In addition, some researchers have suggested a β-sheet conformation in the TM2 domain of $P2X_2$. These data led us to investigate a new architecture within the P2X receptor family. $P2X_7R$ is considered an intriguing receptor because its activation induces nonselective large pore formation, in contrast to the majority of other ionic channel proteins in mammals. This receptor has two states: a low-conductance channel (~10 pS) and a large pore (>400 pS). To our knowledge, one fundamental question remains unanswered: Are the $P2X_7R$ channel and the pore itself the same entity or are they different structures? There are no structural data to help solve this question. Thus, we investigated the hydrophobic M2 domain with the aim of predicting the fitted position and the secondary structure of the TM2 segment from human $P2X_7R$ ($hP2X_7R$). We provide evidence for a β-sheet conformation, using bioinformatics algorithms and molecular-dynamics simulation in conjunction with circular dichroism in different environments and Fourier transform infrared spectroscopy. In summary, our study suggests the possibility that a segment composed of residues from part of the M2 domain and part of the putative TM2 segment of $P2X_7R$ is partially folded in a β-sheet conformation, and may play an important role in channel/pore formation associated with $P2X_7R$ activation. It is important to note that most nonselective large pores have a transmembrane β-sheet conformation. Thus, this study may lead to a paradigmatic change in the $P2X_7R$ field and/or raise new questions about this issue.

INTRODUCTION

P2XRs are a family of ATP-gated ion channels with seven subtypes: $P2X_1$–$P2X_7$. They are ligand-gated ion channels, each with distinct pharmacological and/or physiological properties (6). All seven different subtypes of this receptor family have been found to form functional receptor-ion channel complexes in homo- and/or heterooligomeric assemblies. Within the P2XR family, $P2X_7R$ has particular features and functions (2). This receptor is primarily localized to epithelial and immune cells (3,4). Additionally, current biochemical evidence suggests that $P2X_7R$ has three or six subunits (5,6) and forms a heteromeric association with $P2X_4R$ subunits (7). Its activation in homomeric assembly requires concentrations of ATP that are 10–100 times higher than those required to activate other P2XRs, and the agonist affinity and maximum response can also be modulated 5- to 100-fold by alterations in external monovalent and divalent cations (2,8–10). Moreover, the $P2X_7R$ has other peculiar characteristics, such as a C-terminal tail that is 200 amino acids longer than that of other P2XRs, and the intriguing capacity to form a pore permeable to molecules up to 900 Da (2).

The time course of activation and deactivation of whole-cell currents evoked by activation of recombinant $P2X_7R$ or native $P2X_7$-like receptors varies greatly with species, agonist concentration, duration of agonist application, and different concentrations of divalent cations, such as Ca^{2+} or Mg^{2+} (11). Repeated long-term agonist stimulations have been found to elicit almost constant whole-cell current amplitudes (12,13), successively increasing currents (13–17), or decreasing current amplitudes (15,17,18). These quite different findings have been attributed to activation-dependent, long-lasting changes in $P2X_7R$ conformation; activation of ion channels triggered downstream of the $P2X_7R$ (11); or the existence of two distinct ATP activation sites on $P2X_7R$ (19).

Although several biological functions of $P2X_7R$ have been described, little is known about the intrinsic properties of its molecular structure. In this regard, further elucidation of the $P2X_7R$ structure is crucial for the comprehension of its pharmacological properties and to stimulate the development of new drugs, particularly for the treatment of diseases such as leukemia, arthritis, neuropathic pain, and tuberculosis (20–23).

Previously, Rassendren et al. (24) predicted the membrane topology for the amino-acid sequence of the two transmembrane (TM) stretches of P2XRs, a bulk extracellular domain, and cytoplasmic N- and C-termini. The first TM segment (TM1) is close to the N-terminus (residues 30–50 in the $P2X_2$ subunit), and the second TM segment (TM2) begins

Submitted October 1, 2008, and accepted for publication October 15, 2008.

*Correspondence: alveslaa@ioc.fiocruz.br

Pedro Celso Nogueira Teixeira and Cristina Alves Magalhães de Souza contributed equally to this work.

Editor: Francisco Bezanilla.

0006-3495/09/02/0951/13 $2.00

doi: 10.1016/j.bpj.2008.10.043

close to residue 330 (11). Most of the protein is formed by the intervening ectodomain. This domain has five conserved intrinsic disulfide bonds (25,26) as well as charged residues, both of which play a role in ATP binding (27,28) and are close to TM1 and TM2. This topology is novel for ligand-gated channels (29) but is similar to that of some K^+ channels (29–33), amiloride-sensitive Na^+ channel subunits (34,35), proton-gated cation channels (36), and putative mechanosensitive channel subunits of nematodes (37,38).

It has been suggested that, in contrast to other classes of ion-channel receptors, the P2XRs have amino-acid residues that are responsible for the selectivity and permeability of the channels formed by these receptors, which may not be configured as an α-helix (24). This raises the hypothesis of a TM domain formed by some conformation other than α-helix bundles, a configuration common to other classes of ion channels (39,40). However, this profile was not indicated by other predictions made using informatics tools; on the contrary, no helical conformation was observed in such studies (24). In this context, one report showed that it is possible to generate a tridimensional model of the $P2X_3R$ in which its TM1 and TM2 segments display a higher percentage of β-sheet than α-helix (41). Valera et al. (42) showed that the TM2 segment of the rat $P2X_1R$ strongly resembles the H5 signature segment of the K^+ channels. The H5 signature segment has a key role in the selectivity and permeability of K^+ channels, and the internal part of these channels is geometrically structured as a loop (42). However, there is no information regarding the relative arrangement of TM segments within a subunit, or about the quaternary organization of subunits within P2XRs. Different channels, including epithelial Na^+ channels (ENaCs), inward-rectifier K^+ channels (43), and mechanosensitive channels of *E. coli* (MscL) (32,34,37,38,44,45), show the same number of hydrophobic segments as the P2XRs, but these segments are not associated with pore formation with large conductance and low selectivity as they are in $P2X_7$. Nevertheless, there is still a gap in what we know about the molecular structure of the P2XRs. These facts prompted us to study the whole M2 domain using bioinformatics approaches. These approaches provide evidence of a consensus segment (306–318 residues) in the M2 domain in the P2XR family that could serve an important function, e.g., as a selective filter or participating in channel formation.

To study the possible molecular structure of this segment, we synthesized a peptide segment based on the following criteria: 1), conserved hydrophobic residues in the M2 domain; 2), residues in M2 that align with residues related to the channel lumen of $P2X_2R$ (24); 3), participation in channel-pore formation (24); and 4), the capacity to form a cation-selective channel in an artificial bilayer system (see Fig. S1 in the Supporting Material). This final composed peptide, which is referred to as ADSEG (part of the consensus segment of the M2 domain and part of the TM2 segment; see Fig. 2 *A*), was analyzed by means of molecular-dynamics (MD) simulations, circular dichroism (CD), and Fourier transform infrared (FTIR) spectroscopy to determine its likely conformation in amphipathic and hydrophobic environments. Because of the hydrophobic characteristics of the ADSEG peptide residues, two different solvents were chosen to mimic a membrane environment: TFE (2,2,2-trifluoroethanol) and DMSO (dimethylsulfoxide (CH3)2S=O) (46).

This work suggests for the first time (to our knowledge) that this segment, a scarcely studied region, may play an important role in channel/pore formation associated with $P2X_7R$ activation and also exhibits a propensity for adopting β-sheet folding, such as that observed for porins and voltage-dependent anion-selective channels (47–49). Furthermore, the putative TM2 segment may not be configured solely as an α-helix.

MATERIALS AND METHODS

Peptide synthesis

The peptide sequence was FGIRFDILVFGTGGKFDIIQLVVY (ADSEG, residues 313–336). The ADSEG peptide was synthesized by Genemed Synthesis (San Francisco, CA). The peptide was analyzed by high-performance liquid chromatography and mass spectroscopy, and was 95% pure.

Prediction of the membrane-spanning region

The M1 and M2 hydrophobic domains of the $hP2X_7R$ were analyzed using the scales described by Engelman et al. (50), Eisenberg et al. (51), and Kyte and Doolittle (52), and evaluated for their probability of forming TM segments. Subsequently, we used ClustalX (53) to analyze sequence alignment. An interface was written to provide a single environment in which the user could perform multiple alignments, view the results, and, if necessary, refine and improve the alignment.

The computer strategies used to identify the TM segments (TM1 and TM2) were HMMTOP2 (54) and TMHMM2 (55), which use global approaches to determine the statistically most probable topology for the whole protein according to the underlying model; MEMSAT2 (56) and TMAP (57,58), which use combined forms by evaluating global heuristics or other differences in the distribution of the amino acids; and ALOM2 (59) and TMPRED (60), which use local properties to investigate the amino-acid sequences that are more likely to span the membrane (61).

To gain insight into the M2 domain secondary structure, we used the TOPITS PredictProtein server (62), which performs its predictions based on threading.

PRED-TMBB (63) was used in further analyses to confirm predictions regarding the secondary structure. PRED-TMBB is a Web server that is used to predict TM strands and the topology of β-barrel outer-membrane proteins (63). The server returns a score indicating the probability of the protein being an outer-membrane β-barrel protein. It also reports posterior probabilities for TM strand prediction and furnishes a graphical representation of the assumed position of the TM strands with respect to the lipid bilayer. PRED-TMBB is based on a hidden Markov model, a probabilistic model that consists of several states connected by means of transition probabilities, which has a success rate of 88.8% for the classification of outer-membrane proteins (64).

Secondary structure prediction

MD simulation

Following standard procedures for MD simulations, we used GROMACS version 3.3-1 (65) with force field GROMO-96. Before the MD prediction,

the linear sequence of the ADSEG peptide from the hP2X$_7$R was decoded to display the three-dimensional structure in pdb format using WHATIF (66) based on the receptor structure, followed by both α-helix and β-hairpin sequence conformation from the Swiss PDB Viewer program using set backbone Phi, Psi, and Omega tools. The energies of these structures were minimized (steepest descent: 200; three times) and changed to the gro format. Each one was inserted and centralized in a cubic box (periodic boundary conditions), keeping a minimal distance of 0.5 Å between the peptide and the box boundary. Simulations were carried out in the Gibbs ensemble (NPT) at room temperature (T = 300 K) and atmospheric pressure (1 atm) (67). The united atom ffG53a6 force field was used for parametrization (68) of the Gromacs package (65), a modified version of Gromos96 force field (70); explicit solvation for water (SPC model) (71), for DMSO (72), and for a 30% (vol/vol) TFE/water mixture (73), under periodic boundary conditions (cubic box). Particle mesh Ewald (PME; Fourier spacing 1.2 Å, 4th order, and tolerance 10^{-5}) and six to 12 Lennard-Jones potentials were applied to account for Coulomb and van der Waals interactions, with radii of 10 Å and 14 Å, respectively. The LINCS algorithm was applied over all covalent bonds (74). The energy was initially minimized for all the studied systems. Once the systems were equilibrated, 10 ns data collection runs were carried out. Trajectories were saved every 2 ps, resulting in 5000 snapshots. In all simulations the time step was 0.002 ps.

CD spectroscopy

CD data were collected using a JASCO 715 spectropolarimeter. A 0.1 mm pathlength cuvette with 919.5 μM ADSEG peptide in buffer (150 mM KCl and 10 mM Hepes adjusted to pH 7.4) and 57% TFE was used for the CD experiments. Each CD spectrum was obtained from an average of four scans with a 1-nm bandwidth. The scan rate was 50 nm/min, the step resolution was 0.2 nm, and the response time was 8 s. After background subtraction and smoothing, all CD data were converted from CD signal (millidegrees) into mean residue molar ellipticity (deg cm^2 dmol^{-1}) using the equation $[\theta] = \theta 10^{-1}.l^{-1}.c^{-1}$, where l is the cell length in cm and c is the molar concentration. Analyses of ADSEG peptide for integration into lipid vesicles were performed using two different lipid preparation: phosphatidylethanolamine (PE; Sigma, Berlin, Germany), and *E. coli* polar extract (Avanti Polar Lipids, Alabaster, AL) at 10 mg/mL and 4 mg/mL, respectively. All of the experiments were performed at room temperature (20°C).

Analyses of secondary structure

Deconvolutions were applied to interpret the CD data in terms of secondary structure. Quantitative estimates of the secondary-structure contents were made using the CDPro software package, which includes the programs CONTINLL, CDSSTR, and SELCON3 (75). All three methods were comparable in terms of performance, despite the differences in the algorithms used in the three software packages. Whereas CDSSTR performed best with a smaller reference set and larger wavelength range, and CONTINLL performed best with a larger reference set and smaller wavelength range, the results for individual secondary structures were mixed (75). SELCON3 is the latest version of the self-consistent method SELCON (76). In the self-consistent method, the spectrum of the protein analyzed is included in the matrix of CD spectral data, and an initial guess, considering the structure of the reference protein that has the CD spectrum most similar to that of the protein analyzed, is made for the unknown secondary structure. Analyzing protein CD spectra using all three methods should improve the reliability of predicted secondary structural fractions.

FTIR spectroscopy

FTIR spectra were collected on a Nicolet Magna-IR 760 FT instrument (Nicolet, Madison, WI). The spectral analysis was performed with the OMNIC software provided by the manufacturer. The ADSEG peptide was dissolved in DMSO.

RESULTS

Prediction of the membrane-spanning region

According to the literature, the topology of the P2XRs is predicted as two TM domains (77). To identify these domains, we analyzed the primary sequence of P2X$_7$R with regard to the hydrophobicity of its residues using three different scales as described by Engelman et al. (50), Eisenberg et al. (51), and Kyte and Doolittle (52). The putative TM domains (M1 and M2) according to these scales are shown in Fig. 1. The results displayed on the scales are according to the topology predicted for the P2XRs in the literature, and there is also good agreement among the results from the three scales. The ''break region'' shown in the three scales is a region rich in glycines, which correspond to the 320–326 (LVFGTGG) residues in the M2 domain. This region shows low hydrophobicity and thus provides favorable conditions for loop formation, which is a characteristic of β-hairpin structures (69).

Our next step was to seek a consensus segment in P2XRs in the hydrophobic M2 domain, using ClustalX alignment. The result from this alignment provides a consensus segment (306–318 residues) that contains residues with 100% identity among all P2X$_7$ subtypes (see *blue* residues in Fig. 2 *A*). We also evaluated whether a region of the M2 domain could be folded as an α-helix and participate in the TM2 segment. In this context, we used different approaches for predicting the membrane-spanning region to evaluate the presence α-helix structures in hP2X$_7$R TM1 and TM2. The predictions for the putative topology of TM segments configured as an α-helix are summarized in Tables 1 and 2. The TMHMM2 predicts with high probability only one α-helix TM segment (TM1) for the M1 region of the hP2X$_7$R. HMMTOP2 shows three putative α-helix TM segments—one in the M1 domain

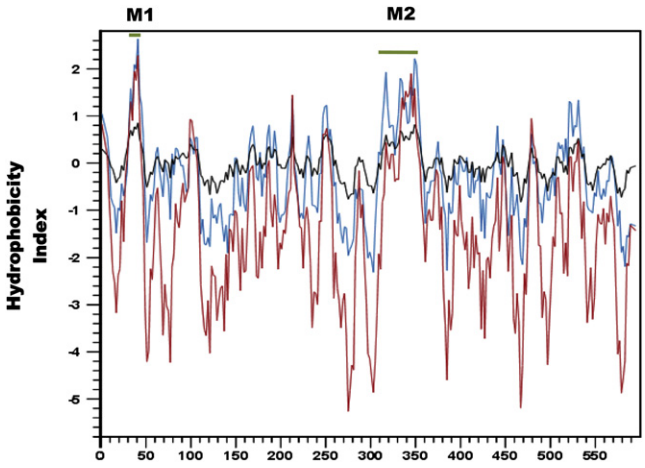

FIGURE 1 Hydrophobicity plot of hP2X$_7$R. Hydrophobicity values were calculated according to three different scales: Engelman (*red*), Eisenberg (*black*), and Kyte and Doolittle (*blue*), and are plotted against the amino-acid sequence (window 21). M1 and M2 (*green line* labeled) indicate the peaks of the putative highly hydrophobic TM regions of hP2X$_7$R.

A

```
H5                                  TATTVGYG
P2X1  GTNYRHLFKVFGIRFDILVDGKAGKFDIIPTMTTIGSGIGIFGVATVLCDLLLLHIL
P2X2  GTTTRTLIKAYGIRIDVIVHGQAGKFSLIPTIINLATALTSVGVGSFLCDWILLTFM
P2X3  GSEYRTLLKAFGIRFDVLVYGNAGKFNIIPTIISSVAAFTSVGVGTVLCDIILLNFL
P2X4  GNEQRTLIKAYGIRFDIIVFGKAGKFDIIPTMINIGSGLALLGMATVLCDIIVLY-
P2X5  GVEFRTLMKAYGIRFDVMVNGKGAFFCDLVLIYLIKKREFYRDKKYEEVRGLEDSSQ
P2X6  GVEARTLLKLYGIRFDILVTGQAGKFGLIPTAVTLGTGAAWLGVVTFFCDLLLLYVD
P2X7  -VEKRTLIKVFGIRFDILVFGTGGKFDIIQLVVYIGSTLSYFGLAAVFIDFLIDTYS
          303        313                 336                  359
                     ADSEG peptide
```

FIGURE 2 ClustalX multiple alignments of the M2 region from the P2XR linear sequences and the H5 signature segment of K^+ channels. (*A*) Green residues are paired with the H5 signature segment (also in *green*); blue residues indicate highly conserved M2 residues; and red boxes show the residues predicted by MEMSAT2 to be configured as a TM α-helix (matrix Blosum 62, gap opening 10.0, and gap extension 1.0). The ADSEG peptide is underlined in red. (*B*) Scheme of the ADSEG peptide region represented in red within the whole $P2X_7R$.

B

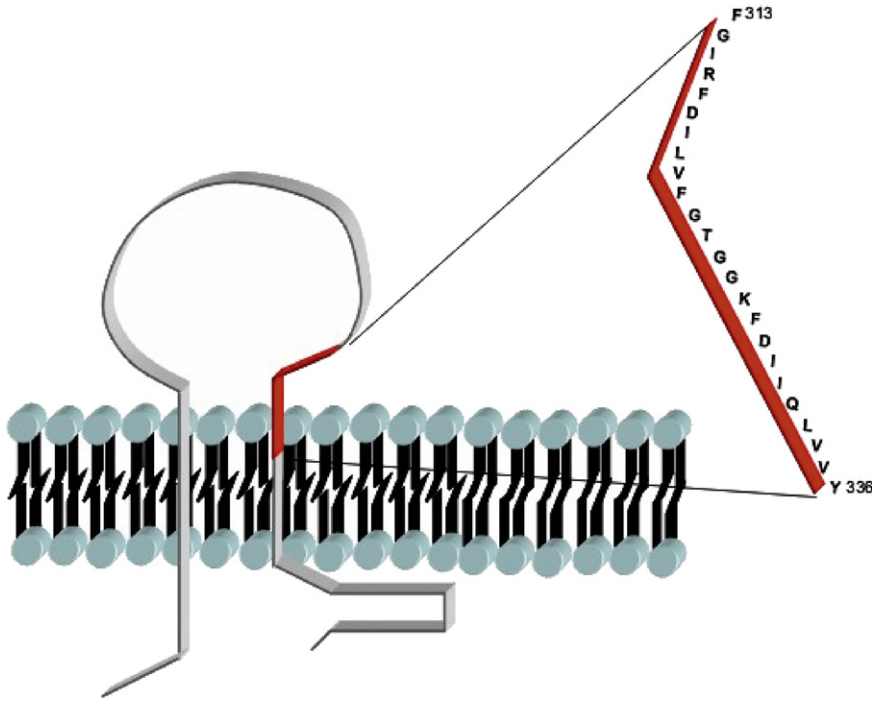

TABLE 1 Summary of predictions of α-helix transmembrane (TM) domains of the $hP2X_7R$

Methods	TM1	TM2	TM3	% accuracy
TMHMM2	25–47	—	—	93.1
HMMTOP2	25–47	309–327	334–356	94.4
MEMSAT2	31–47	333–355	—	91.6
TMAP	29–55	316–344	—	92.9
ALOM2	31–47	—	—	80.1
TMPRED	29–46	333–351	—	93.8

The methods for prediction of transmembrane domains were used according to the following approaches: global approaches—TMHMM2 and HMMTOP2 (based on Hidden Markov Model); local properties—ALOM2 (hydrophobicity-based prediction of membrane helices using a discriminant function) and TMPRED (membrane prediction based on statistical preferences); and combined forms—MEMSAT2 (dynamic programming optimization to find the most likely prediction based on statistical preferences) and TMAP (statistical preferences averaged over aligned profiles). Each program is rated in % accuracy (1). (—) represents negative prediction.

(TM1) and two (TM2 and TM3) in the M2 domain, where TM2 (309–327) is localized in part of the M2 consensus region. ALOM2 confirms the TMHMM2 predictions. MEMSAT2 and TMPRED show two TM domains in the α-helix—TM1 (31–47) and TM2 (333–355)—in the M1 and M2 domains, respectively, where the consensus region does not contain the putative TM2. Similarly to MEMSAT2 and TMPRED, TMAP identifies two TM segments in the α-helix: TM1 and TM2. However, in this case, TM2 (316–344), in contrast to the MEMSAT2 and TMPRED predictions, is also located in the part of the M2 consensus region and plays a role as an integral part of the whole structure. According to these analyses, all programs predict a TM α-helix for the M1 domain; the same was not observed for the M2 domain. Moreover, there are differences in the results regarding the possibility of TM2 assuming an α-helix conformation in this region (TMHMM2 and ALOM2), and

TABLE 2 TOPITS predictions-based threading for the M2 domain of hP2X$_7$R

TOPITS alignments header: summary									
RANK	EALI	LALI	IDEL	NDEL	ZALI	PIDE	LEN2	ID2	NAME 2
1	27.47	53	18	7	2.58	42	109	1mslA	mechanosensitive
10	24.80	54	10	4	2.01	35	158	1gpr	glucose permease

Two of 20 proteins presented by TOPITS were selected by their transmembrane characteristics - the first was the first in rank (an ionic channel protein) and the second was the tenth in the rank (domain A of glucose permease protein). RANK: rank in alignment list, sorted according to z-score; EALI: alignment score; LALI: length of alignment; IDEL: number of residues inserted; NDEL: number of insertions; ZALI: alignment z-score; note: 3>ZALI>0: 1st hit correct in 33% of cases; PIDE: percentage of pairwise sequence identity; LEN2: length of aligned protein structure; ID2: PDB identifier of aligned structure; NAME2: name of aligned protein structure.

also with respect to the possible localization of this segment (MEMSAT2 and TMAP), and the number of segments that form a TM α-helix (HMMTOP2).

We further reevaluated the sequence similarity between the H5 signature segment of the K^+ channel and P2XRs family. The H5 signature segment is crucial for cation selectivity in K^+ channels (42). It is interesting to note that the residues in M2 sequences of the P2XR family that can be aligned with the H5 signature segment (42) resemble a sequence predicted by MEMSAT2 to form an α-helix in TM2 (Fig. 2 *A*, residues in *box*).

It is intriguing that there is a close sequence identity between the H5 signature segment (56%) and the residues in P2X$_1$R (78) and those in P2X$_2$R that are related to channel lumen formation (24). Moreover, it should be pointed out that the H5 signature segment does not form an α-helix (24). This result suggests a possible structural correlation between these regions and the H5 signature segment, which is structurally conformed as a loop in K^+ channels and also acts as a selective filter (79). The scheme in Fig. 2 *B* shows the region corresponding to the ADSEG peptide. It is formed by a large portion of the consensus sequence (*blue residues* in Fig. 2 *A*) and includes some of the residues similar to the H5 signature segment. As mentioned above, the ADSEG peptide forms a cation channel in artificial bilayers (Fig. S1).

Secondary structure prediction for the M2 hP2X$_7$R domain was based on the above-mentioned predictions together with a previous search in PSI-BLAST (data not shown) to find sequences similar to M2 as assessed by TOPITS alignments. TOPITS selects protein sequences that align with the M2 domain not only by pairing residues, but also by testing for a predicted similarity in secondary structure. The results from PSI-BLAST converged on an M2 domain inside the P2XR family itself, and the TOPITS predictions showed 20 proteins with homologous sequences. Two of these were selected based on the fact that they are membrane proteins: one was the first in the rank and corresponds to a mechanosensitive channel protein (1mslA) (80), and the second was the 10th in the rank and corresponds to a glucose permease (1gpr) (81). Fig. 3, *A* and *B*, show molecular structural images of the A domain of mechanosensitive channels (1mslA) (80) and the glucose permease (1gpr) (81), respectively. In these models, the M2 domain aligns with both proteins, and the residues that align with the ADSEG segment are shown in light blue. These protein segments are located in the portion that has a β-sheet conformation

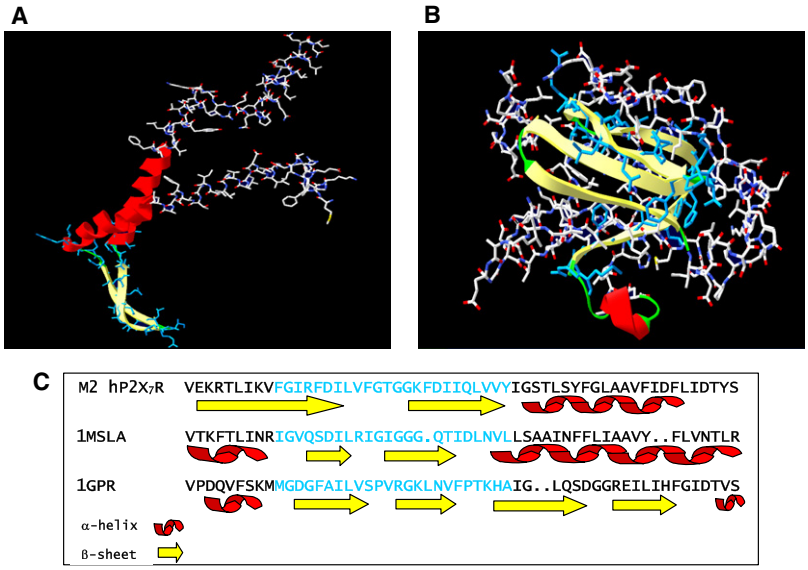

FIGURE 3 Comparison of hP2X$_7$R with other membrane proteins. Images are drawn using the Swiss PDB Viewer program and aligned using TOPITS. (*A*) Domain A of the mechanosensitive channel of high conductance (id - 1mslA). Residues in blue represent the ADSEG peptide, aligned with the β-sheet region of 1-mslA. (*B*) Domain A of the glucose permease (id - 1gpr). Residues in blue represent the ADSEG peptide, also aligned by TOPITS with a β-sheet region of 1gpr. (*C*) Residues in the box represent the TOPITS threading alignments for the M2 domain of hP2X$_7$R with 1mslA and 1gpr. The first line shows the M2 domain of hP2X$_7$R; light blue residues correspond to the ADSEG peptide. The second line shows the 1MslA sequence; light blue residues are paired with the ADSEG peptide. The third line shows the 1gpr sequence; light blue residues are paired with the ADSEG peptide. The residues (*light blue*) correspond to the α-helix (*red*), and β-sheet (*yellow*) structures are indicated below the corresponding sequences.

in Fig. 3 *C*. The high hydrophobicity of the ADSEG peptide and its alignment with an ionic channel (1ms1A) suggest that this segment plays an important role in the channel structure formation of P2XRs. Thus far, these results suggest that the TM2 segment may not be configured solely as a TM α-helix. Based on current findings for the TM2 segment, we suggest that a primary structural model (similar to 1mslA) with the ADSEG peptide can be inserted into the membrane.

Prediction of TM β-strands

Based on the PRED-TMBB program, the M2 domain and the ADSEG peptide sequences produced scores of 2.961 and 2.870, respectively, which are lower than the threshold value of 2.965. The prediction of the TM strands according to posterior decoding using the Viterbi algorithm (VI) is shown in Fig. 4. The posterior probabilities for the TM strands for both segments are shown in Fig. 4, *B* and *D*. The sequences in blue for the M2 domain (15–27 and 55–56 residues in Fig. 4 *A*) and ADSEG peptide (10–18 residues in Fig. 4 *D*) β-strand predictions showed that these residues are similar to that of outer-membrane proteins with a β-barrel topology. The PRED-TMBB predicts a high probability (0.9–1) of a β-sheet conformation for residues (10–18 residues in Fig. 4 *D*) for the ADSEG peptide.

Secondary structure prediction

Structural MD behavior

MD simulations were used to analyze the preferred secondary structure of the ADSEG peptide after exposure of α-helix and β-sheet conformations to DMSO and to a TFE/water mixture. Snapshots of the initial conformations for both structures (α-helix and β-sheet) are shown in Fig. 5, *A* and *B*. The last frames from the DMSO and TFE/water mixture simulations of the two structures (α-helix and β-sheet) are reproduced in Fig. 5, *C–F*. The β-sheet structure after 10 ns simulation in both solvent environments (Fig. 5, *D* and *F*) shows that the initial conformation has a tendency to remain preserved for a longer period. In contrast, the α-helix structure does not show this tendency in the presence of DMSO (Fig. 5 *C*). However, Fig. 5 *E* shows that, in a TFE/water mixture, the α-helix structure remains

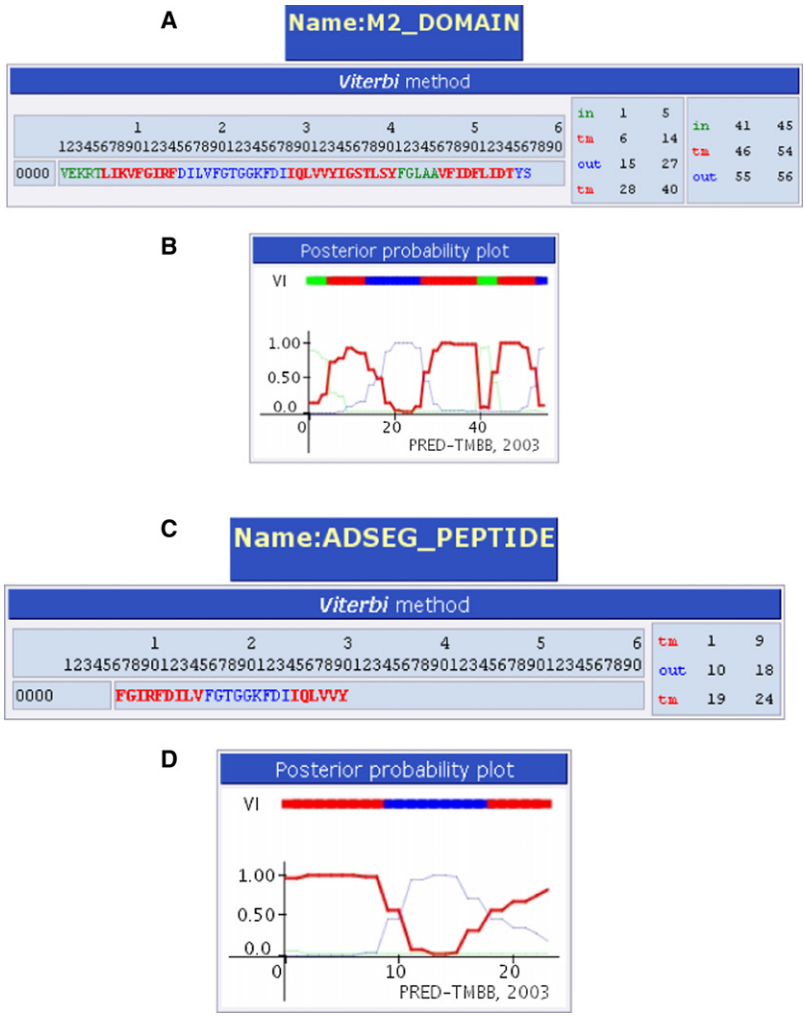

FIGURE 4 Predictions for the TM β-sheet, showing the output of the whole M2 domain prediction obtained from PRED-TMBB (*A* and *B*) and plots of the posterior probabilities for TM strands along the given sequence (*A* and *C*). The sequence score value of the M2 domain was 2.961, which is lower than the threshold value of 2.965. (*D–F*) The same representations of the prediction for the ADSEG peptide. The sequence score value was 2.870, which is lower than the threshold value of 2.965. The difference between the sequence score and the threshold indicates the possibility of the protein being an outer-membrane protein. The residue colors (*green* = in, *red* = TM, and *blue* = out) represent the position of each one in relation to the membrane for the M2 domain (*A*) and ADSEG peptide (*C*), respectively. In *B* and *D*, the green, red, and blue lines show the probability of the residues be β-strand TM (0–1.0) in the *y* axis; the numbers in the *x* axis represent the position of the residues in the M2 domain (56 residues) and ADSEG peptide (24 residues) according to the segment size. To decode the initial amino acid frequencies, the Viterbi (VI) algorithm was used in *B* and *D*.

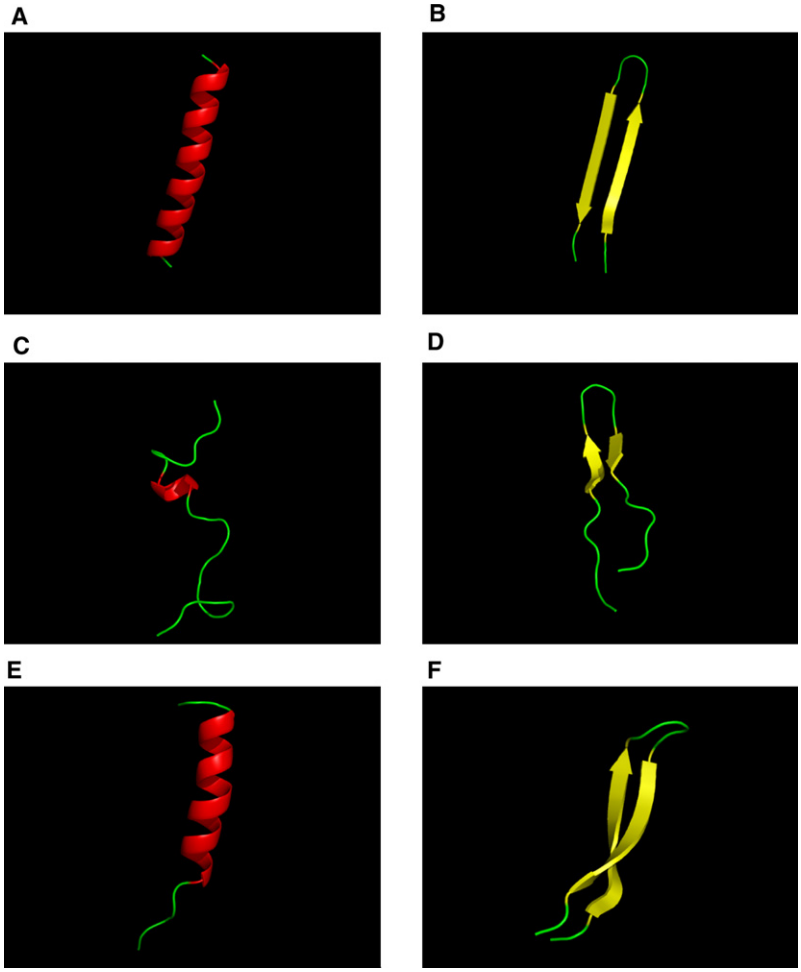

FIGURE 5 Snapshots of the ADSEG peptide starting from an initial conformation of α-helix (*A*) or β-sheet (*B*) and after 10 ns of MD simulations performed in DMSO and a TFE/water mixture. (*C*) α-Helix simulations in DMSO. (*E*) α-Helix simulations in the TFE/water mixture. (*D*) β-Sheet simulations in DMSO. (*F*) β-Sheet simulations in the TFE/water mixture.

closer to its initial conformation throughout the simulation time course.

To characterize the structural evolution of the ADSEG peptide with time, we analyzed the evolution of dihedral angles (φ, ψ) through a 10 ns simulation, assuming that the ADSEG peptide starts as an α-helix or a β-sheet conformation. Fig. S2, *A–D*, represents the Ramachandran plots for α-helix and β-sheet conformations in DMSO and a TFE/water mixture from t = 0 in time intervals of 2 ns to t = 10 ns. In DMSO after 2 ns the initial α-helix conformation shows a tendency for the dihedral angles to scatter from the α-helix region to the β-sheet region in the temporal sequence (Fig. S2 *A*). However, the same behavior was not observed in TFE/water mixture (Fig. S2 *C*). When the simulations started from a β-sheet structure in DMSO or the TFE/water mixture, the evolution of the dihedral angles showed a tendency to remain in the region favorable to a β-sheet conformation (see time intervals in Fig. S2, *B* and *D*).

A detailed analysis of the time evolution of dihedral angles (0–10 ns) displayed in Fig. S2 *A–D* revealed the following findings: 1) In DMSO, 79% of the residues originally distributed in the α-helix region are scattered; however, 26% of these residues (79%) are now localized in the β-sheet region (Fig. S2 *A*). Nevertheless, after starting from the β-sheet conformation (in DMSO), most of the residues (67%) still appear in the original β-sheet region (Fig. S2 *B*). 2) In the TFE/water mixture starting from the β-sheet conformation (Fig. S2 *D*), 81% of the residues remain in the β-sheet region; however, after starting from the α-helix conformation in the TFE/water mixture (Fig. S2 *C*), 75% of the residues remain in the α-helix region. Only a few residues (17%) are displaced from the α-helix region to the β-sheet region.

The backbone root mean-square (RMS) deviation values with respect to the initial structure for each of the two structures (α-helix and β-sheet) in both organic solvents as a function of time are reported in Fig. 6. In both solvents the β-sheet structure remains closer to its starting conformation. Regarding the α-helix structure, a significant increase occurs in the RMSD values in DMSO (Fig. 6), indicating a rapid divergence from the starting conformation up to 1 ns of simulation. After ~3 ns, we calculated the RMSD mean values that developed from the α-helix and β-sheet structures in the presence of both solvents. The RMSD mean value starting from a helical structure in DMSO was 0.75 nm, which was much higher than the mean values

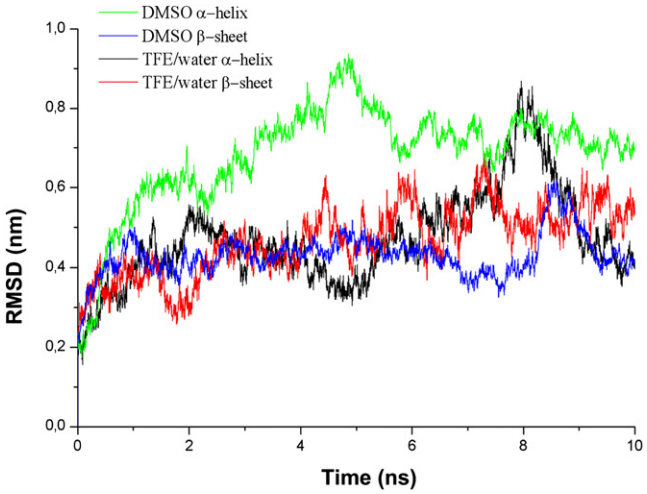

FIGURE 6 Time evolution (in nanoseconds) of the backbone RMS deviation (in nm) during simulation of the ADSEG peptide with respect to the minimized initial structure for α-helix and β-sheet structures. Shown are the α-helix (*green line*) and β-sheet (*blue line*) in DMSO, and the α-helix (*black line*) and β-sheet (*red line*) in the TFE/water mixture.

(~0.4 nm) obtained from the helical structure in the TFE/water mixture, and from the β-sheet structure in both solvents. Starting from the β-sheet structure in DMSO, the mean value reached only 0.4 nm. The increase in the RMSD value in DMSO indicates a greater change from the initial α-helix structure, as observed in Ramachandran plots during the time evolution of dihedral angles (Figs. S2 *A* and 6). In contrast, its behavior in the TFE/water mixture shows a propensity for maintaining the α-helix structure population in the favorable α-helix region (Fig. S2 *C*); the RMSD values remained low (0.5 nm). With respect to the β-sheet structure in the TFE/water mixture, its structure remained defined and no significant increase occurred; the RMSD mean value was 0.5 nm. This result is in agreement with reports in the literature indicating that TFE works as a strong cosolvent that stabilizes α-helix and β-sheet structures in a variety of peptides and proteins. The same behavior was observed in the DMSO simulations, where the β-sheet structure remained well defined throughout the 10 ns simulation (Fig. S2). These results indicate that the β-sheet structure is more preserved than the α-helix in both environments.

Secondary structure evaluated by CD spectroscopy

To validate the bioinformatics data, we analyzed CD spectra of the ADSEG peptide in different environments. CD spectroscopy is a useful technique for studying secondary structure and the folding and binding properties of proteins and peptides (82). The structural behavior of the ADSEG peptide in vesicles of different compositions is shown in Fig. 6. The spectrum obtained for the peptide in the presence of TFE indicates preferential self-folding into a β-sheet conformation rather than an α-helix (Fig. 6). Of interest, the predominance of this typical β-sheet conformation was demonstrated with the ADSEG peptide in free form as well as incorporated into vesicles. The peptide conformations were not affected by incorporation into vesicles or by solvent composition. There were no changes in the β-sheet content when the ADSEG peptide was incorporated into the PE or *E. coli* polar extract. The *E. coli* polar extract consists mainly of zwitterionic phospholipid PE (70–75%) and two anionic phospholipids: phosphatidylglycerol (PG, 20–25%) and cardiolipin (CL, 5–10%) (83). The experiments performed in the artificial planar lipid bilayer with the ADSEG peptide showed that there was no peptide insertion when PE was used as a lipid membrane, although different results were found using *E. coli* polar extract (data not shown).

Analyses of secondary structure by CD spectroscopy

The results shown in the inset of Fig. 7 are related to the values from the package of deconvolution algorithms used (CONTINLL, CDSSTR, and SELCON3). The secondary structure contents estimated by all three deconvolution algorithms showed a higher β-sheet content than the content of α-helix (Fig. 7, *inset*) for the ADSEG peptide. There were no changes in β-sheet content even when the ADSEG peptide was incorporated into PE or *E. coli* polar extract vesicle, indicating that the incorporation into different lipid vesicles did not affect the β-sheet content.

It is important to point out that TFE is a useful solvent for studying peptides and protein fragments by CD (84). On the other hand, DMSO has been described as a solvent that is not convenient for far-UV CD experiments because it absorbs strongly below 240 nm, thereby preventing the extraction of secondary structure contents from CD spectra (82). However, the MD simulations were sufficient to obtain detailed ADSEG peptide secondary structures in the presence of DMSO (Fig. 5, *C* and *D*).

FTIR analyses

To overcome the problems of analyzing the secondary structure of the ADSEG peptide dissolved in DMSO by CD, we performed FTIR experiments. FTIR has been widely used to study protein and peptide conformations (85). Because sample absorption is not a problem in this case, since only molecular vibrations are measured, we were able to use DMSO (86). The analysis of the amide I band indicates a mixture of α-helix and β-sheet configuration (Fig. S3), reinforcing the data obtained by MD, which showed a major propensity for β-sheet conformation. It is possible that equilibrium among peptide conformations is achieved rapidly. However, the MD simulations revealed a preferential conformation adopted by this peptide. Thus, the FTIR data are in agreement with the results described above and reinforce the suggestion about a major probability to observe a β-sheet over α-helix conformation.

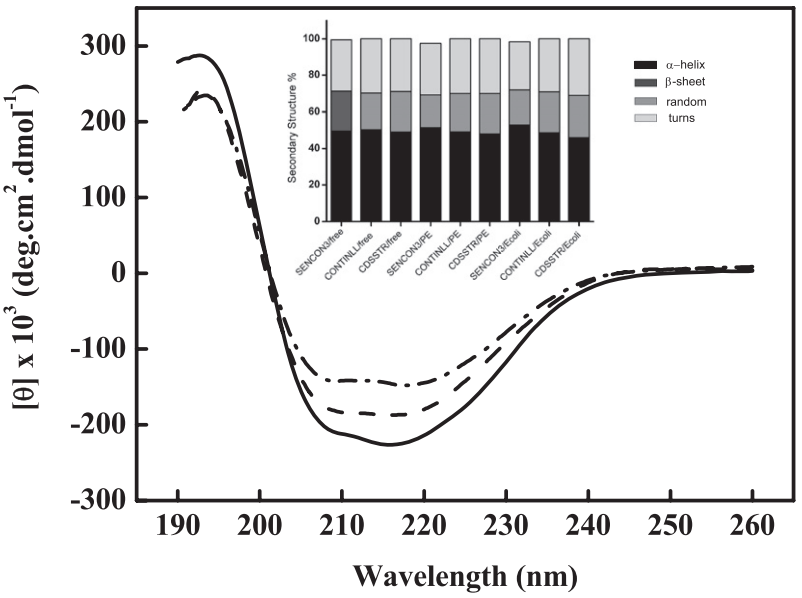

FIGURE 7 CD spectra of the ADSEG peptide and deconvolution analyses of the secondary strutcture. The peptide is shown in the absence (*solid line*) and presence of lipid vesicles composed of PE (*dashed line*) or lipids extracted from *E. coli* (*dotted-dashed line*). The vesicles and ADSEG peptide concentrations were 10 mg/mL and 919.5 μM, respectively. The inset shows the relative amounts of each secondary structure element, estimated using CONTINLL, CDSSTR, and SELCON3. The first, second, and third groups of the deconvolution algorithms refer to free, PE, and *E. coli* lipid vesicle environments, respectively.

DISCUSSION

The scarcity of crystallographic and NMR studies of P2XRs architecture makes it difficult to understand its structural arrangements, as well as its stoichiometry and pharmacological profiles. The aim of this study was to investigate the molecular structure of part of the hydrophobic M2 domain of $P2X_7R$. To attain this objective, different bioinformatics approaches and experimental tools were used. In contrast to other ligand-gated ion channels, the putative TM2 segment of the P2XRs demonstrates great variability among the different subunits of the residues of that segment. The absence of primary sequence conservation among the P2X subunits of all P2XR subtypes makes it difficult to identify those segments that constitute the internal part of the channel (24). Some findings indicate that TM2 resembles similar domains of other ionic channels in its potential to form an amphipathic α-helix having a hydrophilic face that lines part of the water-filled ion-conducting pore (87). To date, to our knowledge, there are no conclusive data showing either the specific segment of $P2X_7R$ lining the pore or its molecular structure.

In this study, we analyzed the M2 domain and ADSEG peptide in $hP2X_7R$ by employing bioinformatics approaches, MD, CD, and FTIR to evaluate the possible conformation and position of the TM segment. The first step was to confirm the topology of the two putative TM domains of the $hP2X_7R$. The hydrophobicity plots of the $hP2X_7R$ identified the putative highly hydrophobic TM regions (M1 and M2), confirming the literature findings (77).

The predictions for the TM segment in the M2 domain were obtained using different bioinformatics approaches with different high accuracy algorithms. These predictions show that there are discrepancies among the results from different programs as regards the location of TM in the M2 domain, and these discrepancies cast doubt on the hypothesis that this region is configured as a TM α-helix. Reinforcing this suggestion, Egan et al. (88) have also shown that the TM2 may not be stable as an α-helix. On the other hand, the literature describes the majority of TM proteins and ion-gated channels as being configured as an α-helical bundle (39). Despite the α-helix paradigm regarding formation of the conducting pore of the ionic channels, there are some membrane proteins, such as porins, that are configured as β-pleated sheets in the form of a closed barrel and that function as ion-gated channels (48,49). Of interest, TM β-barrels are found not only in outer-membrane proteins (e.g., OmpA, OmpX, phospholipase A, general and substrate-specific porins, and TonB-dependent receptors), but also in several toxins that assemble on the membrane to form oligomeric TM channels, such as the heptameric pore-forming α-hemolysin from *Staphylococcus aureus*, the human voltage-dependent anion-selective channels (89), and the cation-selective pore Tom40 from human mitochondria outer membrane (90).

Although several different Web-based predictors for α-helical membrane proteins are currently available, there is no freely available prediction method for β-barrel membrane proteins, at least not with an acceptable level of accuracy (63). In the study presented here, the reports from PRED-TMBB analyses using the M2 domain and ADSEG peptide produced a score lower than the threshold value, indicating the possibility that the ADSEG peptide is a β-barrel membrane protein (Fig. 5, *C* and *D*).

Taken together, our results are consistent with the possibility that the ADSEG peptide composes the TM structure of the channel, since it is preferentially configured as a β-sheet. In this context, the MD, CD, and FTIR analyses

of the ADSEG peptide were essential to corroborate our hypothesis.

MD simulations are used to elucidate molecular structures and to gain insight into the natural dynamics of biomolecules in solution on different timescales. Here, we attempted to simulate the behavior of the ADSEG peptide in two membrane-mimetic solvents—DMSO and a TFE/water mixture—using MD simulations (46,91). DMSO, a powerful organic solvent with amphipathic characteristics, is widely used in cell biology because of its ability to induce cell fusion and cell differentiation, increase membrane permeability, and change protein properties (72). Leu-enkephalin in DMSO shows a well-defined conformation, making it possible to compare the zwitterionic and the neutral forms (92). A model for the 3D structure of an analog of oxytocin antagonist (OT-BC) was proposed based on MD simulations in DMSO (93). The solution structure of OT-BC was consistent with structure-activity relations of peptide and nonpeptide antagonists of oxytocin (OT). In particular, they also revealed that a β-turn was the common feature responsible for antagonist interaction with the uterine receptor of OT. Another important finding was reported by Bennett et al. (94). They demonstrated by MD simulations in DMSO that six (TM2, TM7–TM11) TM segments from lactose permease (LacY) retained a significant (>20%) secondary structure for the duration of the simulation. Those results were in substantial agreement with NMR data published previously. Moreover, MD simulations of a fragment of gp120 (envelope protein of HIV-1) in DMSO reveled a β-sheet structure (95). According to the data described above, and taking into account our findings using MD simulations in DMSO as a membrane-mimic solvent, we can say that this solvent can be used either for hydrophilic or hydrophobic proteins, in agreement with the amphipathic characteristics of this solvent.

TFE has also served as a nonpolar cosolvent in studies of conformation equilibrium and protein-folding kinetics (96,97). Although TFE is fully miscible with water at any ratio, the molecule forms microscopic clusters in aqueous solutions with the greatest propensity for aggregation near 30 vol %, the optimal concentration for inducing secondary structure stabilization in peptides and proteins (98). At these concentrations, TFE strongly stabilizes the α-helix and β-sheet structures of many soluble and amphiphilic peptides. The effect of TFE on peptides is most likely due to its ability to effectively coat the surface of the peptide. By aggregating around the solute, the TFE molecules exclude water, favoring the formation of intramolecular hydrogen bonds and promoting the formation of secondary structure (99,100). The effect of TFE on the stability of α-helix-forming peptides has been investigated by several authors (101). According to our MD simulations analyzed by Ramachandran plots displayed as function of the time evolution of the dihedral angles (φ, ψ) and RMSD calculations, in both DMSO and a TFE/water mixture, the β-sheet structure is almost unchanged from its original secondary structure for at least 10 ns, whereas the α-helix structure has a tendency to scatter from the favored α-helix region in Ramachandran plots in the presence of DMSO. Additionally, some of the scattered residues (in the α-helix region) converged to the favored β-sheet region, whereas fewer residues migrated to the β-sheet region in the TFE/water mixture. Although some fluctuations were observed in the RMSD plots during the simulation, they do not represent significant changes in the secondary structure conformation of the ADSEG peptide (Fig. 6, *B* and *D*). It is important to point out that the RMSD plots show only the rate of deviation from the initial conformation of the ADSEG peptide, without indicating either the stability of the system or the secondary structure. The time simulations on Ramachandran plots show the tendency and secondary structure evolution that the ADSEG peptide can adopt. These results provide clear evidence that the ADSEG peptide exhibits a propensity for adopting the β-sheet fold.

A few studies of sheet-forming peptides in TFE/water mixture have been done. In this work, we found a β-sheet structure in the presence of TFE as well as an α-helix, as should be expected for this solvent (99,100). However, our results show that the residues of the α-helix structure in a TFE/water mixture have a slight tendency to scatter to the favored β-sheet region. Finally, TFE has been shown to accelerate protein folding (96) and disfavor partially folded intermediates even at low concentrations (97). Serrano et al. (102) showed by MD simulation that a 20-residue peptide was partially folded in a 40% (vol/vol) TFE/water mixture as a β-hairpin. In another study, a 16-residue peptide adopted a stable β-hairpin structure in aqueous solution with a population of ~40% (103).

According to our MD results, the ADSEG peptide preferentially assumes a β-sheet structure rather than an α-helix in both solvents. Rassendren et al. (24) also demonstrated that there is a region in the second hydrophobic domain of the P2XRs that is exposed within the ionic pore. However, this finding does not support the hypothesis that a pore is formed at the polar face of an amphipathic α-helix. Given the large number of residues that react with Ag^+, Egan et al. (88) concluded that TM2 crosses the membrane in a nonhelical manner, and suggested that this domain makes a major contribution to the pore structure. Considering a β-sheet as the initial conformation, our MD ADSEG peptide simulations resulted in a preferential structure for both solvents (Fig. 5, *D* and *F*), whereas the same motif was not observed when we performed the simulations starting from an α-helix structure (Fig. 5, *C* and *E*). Together, these results suggest a possible β-hairpin arrangement in part of the TM2 segment of the $P2X_7R$ similar to those found in some defensins (104).

To experimentally confirm the results obtained from the bioinformatics predictions, we evaluated the ADSEG peptide by CD spectroscopy in different environments. As observed in the MD simulations, the initial peptide structure

(α-helix or β-sheet) was maintained in the TFE/water mixture. The CD spectra showed a mixture of α-helix with β-sheet structures, with β-sheet predominating. These results clearly indicate that the preferential structure assumed by this segment is β-sheet. A similar behavior was observed for the ADSEG peptide in the presence of DMSO. Thus, our experimental data provide good support for the MD results.

It is important to note that the model proposed by our group for part of the M2 domain of $P2X_7R$ with β-sheet structures is not a surprising model for peptides, as other ion channels can have this configuration (48,49). One could imagine that a β-sheet conformation is crucial to high-conductance channels ($>$ 400 pS) since bacterial porins and the human voltage-dependent anion-selective channels have conductances above this range. Also, it is possible to speculate that this segment may be responsible for the structure of the ionic channel of the integral $P2X_7R$ in ''large conductance conformation,'' which would be reached when the $P2X_7R$ is activated by high ATP concentrations (millimolars; see Fig. S4). In addition, assuming the presence of β-sheet in the peptide configuration (Fig. S4), the following sequence is quite plausible: When ATP in high concentration is linked to $P2X_7R$, eliciting a cation influx and an intracellular cascade, the β-sheet may assume a configuration that allows passage of molecules up to 1 kDa. In other words, the channel will transiently perform a large pore function due to the presence in that region of this β-sheet segment. This model may allow the coexistence of two functions (channel and large pore) in a single structure. It does not exclude the need of another protein serving a large pore function.

Further investigation is necessary to understand this possible paradigmatic change, i.e., the notion that β-sheet conformation participates in pore formation of $P2X_7R$.

SUPPORTING MATERIAL

Four figures are available at http://www.biophysj.org/biophysj/supplemental/S0006-3495(08)00129-X .

We thank Prof. Vinicius Cotta de Almeida and Prof. Roberto Magalhães Saraiva for helpful discussions and suggestions. We are deeply indebted to Prof. Martha Sorenson, who carefully read the manuscript and gave much needed comments. We also thank Antonio Augusto Fidalgo Neto and Filipe Faria Berçot for drawing the figures. This work was supported by grants from the Instituto Oswaldo Cruz, Fundaçao de Amparo a Pesquisa do Rio de Janeiro, and Millennium Institute for Structural Biology in Biomedicine and Biotechnology (CNPq Millennium Program).

REFERENCES

1. Cuthbertson, J. M., D. A. Doyle, and M. S. Sansom. 2005. Transmembrane helix prediction: a comparative evaluation and analysis. *Protein Eng. Des. Sel.* 18:295–308.
2. Surprenant, A., F. Rassendren, E. Kawashima, R. A. North, and G. Buell. 1996. The cytolytic P2Z receptor for extracellular ATP identified as a P2X receptor (P2X7). *Science.* 272:735–738.
3. Collo, G., S. Neidhart, E. Kawashima, M. Kosco-Vilbois, R. A. North, et al. 1997. Tissue distribution of the P2X7 receptor. *Neuropharmacology.* 36:1277–1283.
4. Mutini, C., S. Falzoni, D. Ferrari, P. Chiozzi, A. Morelli, et al. 1999. Mouse dendritic cells express the P2X7 purinergic receptor: characterization and possible participation in antigen presentation. *J. Immunol.* 163:1958–1965.
5. Nicke, A., H. G. Baumert, J. Rettinger, A. Eichele, G. Lambrecht, et al. 1998. P2X1 and P2X3 receptors form stable trimers: a novel structural motif of ligand-gated ion channels. *EMBO J.* 17:3016–3028.
6. North, R. A., and A. Surprenant. 2000. Pharmacology of cloned P2X receptors. *Annu. Rev. Pharmacol. Toxicol.* 40:563–580.
7. Guo, C., M. Masin, O. S. Qureshi, and R. D. Murrell-Lagnado. 2007. Evidence for functional P2X4/P2X7 heteromeric receptors. *Mol. Pharmacol.* 72:1447–1456.
8. Rassendren, F., G. N. Buell, C. Virginio, G. Collo, R. A. North, et al. 1997. The permeabilizing ATP receptor, P2X7. Cloning and expression of a human cDNA. *J. Biol. Chem.* 272:5482–5486.
9. Michel, A. D., I. P. Chessell, and P. P. Humphrey. 1999. Ionic effects on human recombinant P2X7 receptor function. *Naunyn Schmiedebergs Arch. Pharmacol.* 359:102–109.
10. Gudipaty, L., B. D. Humphreys, G. Buell, and G. R. Dubyak. 2001. Regulation of P2X(7) nucleotide receptor function in human monocytes by extracellular ions and receptor density. *Am. J. Physiol. Cell Physiol.* 280:C943–C953.
11. North, R. A. 2002. Molecular physiology of P2X receptors. *Physiol. Rev.* 82:1013–1067.
12. Bretschneider, F., M. Klapperstuck, M. Lohn, and F. Markwardt. 1995. Nonselective cationic currents elicited by extracellular ATP in human B-lymphocytes. *Pflugers Arch.* 429:691–698.
13. Klapperstuck, M., C. Buttner, T. Bohm, G. Schmalzing, and F. Markwardt. 2000. Characteristics of P2X7 receptors from human B lymphocytes expressed in *Xenopus* oocytes. *Biochim. Biophys. Acta.* 1467:444–456.
14. Ugur, M., R. M. Drummond, H. Zou, P. Sheng, J. J. Singer, et al. 1997. An ATP-gated cation channel with some P2Z-like characteristics in gastric smooth muscle cells of toad. *J. Physiol.* 498:427–442.
15. Kim, M., L. H. Jiang, H. L. Wilson, R. A. North, and A. Surprenant. 2001. Proteomic and functional evidence for a P2X7 receptor signalling complex. *EMBO J.* 20:6347–6358.
16. Chessell, I. P., A. D. Michel, and P. P. Humphrey. 1997. Properties of the pore-forming P2X7 purinoceptor in mouse NTW8 microglial cells. *Br. J. Pharmacol.* 121:1429–1437.
17. Virginio, C., A. MacKenzie, R. A. North, and A. Surprenant. 1999. Kinetics of cell lysis, dye uptake and permeability changes in cells expressing the rat P2X7 receptor. *J. Physiol.* 519:335–346.
18. Petrou, S., M. Ugur, R. M. Drummond, J. J. Singer, and J. V. Walsh, Jr.. 1997. P2X7 purinoceptor expression in Xenopus oocytes is not sufficient to produce a pore-forming P2Z-like phenotype. *FEBS Lett.* 411:339–345.
19. Klapperstuck, M., C. Buttner, G. Schmalzing, and F. Markwardt. 2001. Functional evidence of distinct ATP activation sites at the human P2X(7) receptor. *J. Physiol.* 534:25–35.
20. Zhang, X. J., G. G. Zheng, X. T. Ma, Y. H. Yang, G. Li, et al. 2004. Expression of P2X7 in human hematopoietic cell lines and leukemia patients. *Leuk. Res.* 28:1313–1322.
21. Cabrini, G., S. Falzoni, S. L. Forchap, P. Pellegatti, A. Balboni, et al. 2005. A His-155 to Tyr polymorphism confers gain-of-function to the human P2X7 receptor of human leukemic lymphocytes. *J. Immunol.* 175:82–89.
22. Fernando, S. L., B. M. Saunders, R. Sluyter, K. K. Skarratt, J. S. Wiley, et al. 2005. Gene dosage determines the negative effects of polymorphic alleles of the P2X7 receptor on adenosine triphosphate-mediated killing of mycobacteria by human macrophages. *J. Infect. Dis.* 192:149–155.

23. Franco-Martinez, S., P. Nino-Moreno, S. Bernal-Silva, L. Baranda, M. Rocha-Meza, et al. 2006. Expression and function of the purinergic receptor P2X7 in patients with pulmonary tuberculosis. *Clin. Exp. Immunol.* 146:253–261.
24. Rassendren, F., G. Buell, A. Newbolt, R. A. North, and A. Surprenant. 1997. Identification of amino acid residues contributing to the pore of a P2X receptor. *EMBO J.* 16:3446–3454.
25. Clyne, J. D., L. F. Wang, and R. I. Hume. 2002. Mutational analysis of the conserved cysteines of the rat P2X2 purinoceptor. *J. Neurosci.* 22:3873–3880.
26. Ennion, S. J., and R. J. Evans. 2002. Conserved cysteine residues in the extracellular loop of the human P2X(1) receptor form disulfide bonds and are involved in receptor trafficking to the cell surface. *Mol. Pharmacol.* 61:303–311.
27. Ennion, S. J., S. Hagan, and R. J. Evans. 2000. The role of positively charged amino acids in ATP recognition by human P2X1 receptors. *J. Biol. Chem.* 275:29361–29367.
28. Jiang, L. H., F. Rassendren, A. Surprenant, and R. A. North. 2000. Identification of amino acid residues contributing to the ATP-binding site of a purinergic P2X receptor. *J. Biol. Chem.* 275:34190–34196.
29. Ortells, M. O., and G. G. Lunt. 1995. Evolutionary history of the ligand-gated ion-channel superfamily of receptors. *Trends Neurosci.* 18:121–127.
30. Aldrich, R. 1993. Potassium channels. Advent of a new family. *Nature.* 362:107–108.
31. Rossier, B. C., C. M. Canessa, L. Schild, and J. D. Horisberger. 1994. Epithelial sodium channels. *Curr. Opin. Nephrol. Hypertens.* 3:487–496.
32. Suzuki, M., K. Takahashi, M. Ikeda, H. Hayakawa, A. Ogawa, et al. 1994. Cloning of a pH-sensitive K+ channel possessing two transmembrane segments. *Nature.* 367:642–645.
33. Krapivinsky, G., E. A. Gordon, K. Wickman, B. Velimirovic, L. Krapivinsky, et al. 1995. The G-protein-gated atrial K+ channel IKACh is a heteromultimer of two inwardly rectifying K(+)-channel proteins. *Nature.* 374:135–141.
34. Canessa, C. M., J. D. Horisberger, and B. C. Rossier. 1993. Epithelial sodium channel related to proteins involved in neurodegeneration. *Nature.* 361:467–470.
35. Jentsch, T. J. 1994. Trinity of cation channels. *Nature.* 367:412–413.
36. Waldmann, R., G. Champigny, F. Bassilana, C. Heurteaux, and M. Lazdunski. 1997. A proton-gated cation channel involved in acid-sensing. *Nature.* 386:173–177.
37. Hong, K., and M. Driscoll. 1994. A transmembrane domain of the putative channel subunit MEC-4 influences mechanotransduction and neurodegeneration in *C. elegans*. *Nature.* 367:470–473.
38. Huang, M., and M. Chalfie. 1994. Gene interactions affecting mechanosensory transduction in *Caenorhabditis elegans*. *Nature.* 367: 467–470.
39. Brake, A. J., and D. Julius. 1996. Signaling by extracellular nucleotides. *Annu. Rev. Cell Dev. Biol.* 12:519–541.
40. Popot, J. L., and D. M. Engelman. 2000. Helical membrane protein folding, stability, and evolution. *Annu. Rev. Biochem.* 69:881–922.
41. Mager, P. P., A. Weber, and P. Illes. 2004. Bridging the gap between structural bioinformatics and receptor research: the membrane embedded, ligand-gated, P2X glycoprotein receptor. *Curr. Top. Med. Chem.* 4:1657–1705.
42. Valera, S., N. Hussy, R. J. Evans, N. Adami, R. A. North, et al. 1994. A new class of ligand-gated ion channel defined by P2X receptor for extracellular ATP. *Nature.* 371:516–519.
43. Schwalbe, R. A., C. S. Wingo, and S. L. Xia. 2002. Mutations in the putative pore-forming segment favor short-lived wild- type Kir2.1 pore conformations. *Biochemistry.* 41:12457–12466.
44. Ho, K., C. G. Nichols, W. J. Lederer, J. Lytton, P. M. Vassilev, et al. 1993. Cloning and expression of an inwardly rectifying ATP-regulated potassium channel. *Nature.* 362:31–38.
45. Kubo, Y., T. J. Baldwin, Y. N. Jan, and L. Y. Jan. 1993. Primary structure and functional expression of a mouse inward rectifier potassium channel. *Nature.* 362:127–133.
46. Duarte, A. M., C. P. van Mierlo, and M. A. Hemminga. 2008. Molecular dynamics study of the solvation of an alpha-helical transmembrane peptide by DMSO. *J. Phys. Chem. B.* 112:8664–8671.
47. Shanmugavadivu, B., H. -J. Apell, T. Meins, K. Zeth, and J. H. Kleinschidt. 2007. Correct folding of the beta-barrel of the human membrane protein VDAC requires a lipid bilayer. *J. Mol. Biol.* 368:66–78.
48. Koebnik, R., K. P. Locher, and G. P. Van. 2000. Structure and function of bacterial outer membrane proteins: barrels in a nutshell. *Mol. Microbiol.* 37:239–253.
49. Schulz, G. E. 2002. The structure of bacterial outer membrane proteins. *Biochim. Biophys. Acta.* 1565:308–317.
50. Engelman, D. M., T. A. Steitz, and A. Goldman. 1986. Identifying nonpolar transbilayer helices in amino acid sequences of membrane proteins. *Annu. Rev. Biophys. Biophys. Chem.* 15:321–353.
51. Eisenberg, D. 1984. Three-dimensional structure of membrane and surface proteins. *Annu. Rev. Biochem.* 53:595–623.
52. Kyte, J., and R. F. Doolittle. 1982. A simple method for displaying the hydropathic character of a protein. *J. Mol. Biol.* 157:105–132.
53. Thompson, J. D., T. J. Gibson, F. Plewniak, F. Jeanmougin, and D. G. Higgins. 1997. The ClustalX windows interface: flexible strategies for multiple sequence alignment aided by quality anlysis tools. *Nucleic Acids Res.* 24:4876–4882.
54. Chen, C. P., A. Kernytsky, and B. Rost. 2002. Transmembrane helix predictions revisited. *Protein Sci.* 11:2774–2791.
55. Sonnhammer EL, G. von Heijne, and A. Krogh. 1998. A hidden Markov model for predicting transmembrane helices in protein sequences. *Proc. Int. Conf. Intell. Syst. Mol. Biol.* 6:175–182.
56. Jones, D. T., W. R. Taylor, and J. M. Thornton. 1994. A model recognition approach to the prediction of all-helical membrane protein structure and topology. *Biochemistry.* 33:3038–3049.
57. Persson, B., and P. Argos. 1994. Prediction of transmembrane segments in proteins utilising multiple sequence alignments. *J. Mol. Biol.* 237:182–192.
58. Persson, B., and P. Argos. 1997. Prediction of membrane protein topology utilizing multiple sequence alignments. *J. Protein Chem.* 16:453–457.
59. Nakai, K., and M. Kanehisa. 1992. A knowledge base for predicting protein localization sites in eukaryotic cells. *Genomics.* 14:897–911.
60. Hofmann, K., and W. Stoffel. 1993. TMBASE-a database of membrane spanning protein segments. *Biol. Chem. Hoppe Seyler.* 374:166.
61. Moller, S., M. D. Croning, and R. Apweiler. 2001. Evaluation of methods for the prediction of membrane spanning regions. *Bioinformatics.* 17:646–653.
62. Rost, B. 1995. TOPITS: threading one-dimensional predictions into three-dimensional structures. *Proc. Int. Conf. Intell. Syst. Mol. Biol.* 3:314–321.
63. Bagos, P. G., T. D. Liakopoulos, I. C. Spyropoulos, and S. J. Hamodrakas. 2004. PRED-TMBB: a web server for predicting the topology of beta-barrel outer membrane proteins. *Nucleic Acids Res.* 32:W400–W404.
64. Bagos, P. G., T. D. Liakopoulos, I. C. Spyropoulos, and S. J. Hamodrakas. 2004. A Hidden Markov Model method, capable of predicting and discriminating β-barrel outer membrane proteins. *BMC Bioinformatics.* 5:29.
65. Lindahl, E., B. Hess, and D. van der Spoel. 2001. GROMACS 3.0: a package for molecular simulation and trajectory analysis. *J. Mol. Model.* 7:306–317.
66. Vriend, G. 1990. WHAT IF: a molecular modeling and drug design program. *J. Mol. Graph.* 8:52–56.

67. Berendsen, K., J. Postma, W. F. van Gunsteren, A. DiNola, and J. R. Haak. 1984. Molecular dynamics with coupling to an external bath. *J. Chem. Phys.* 81:3684–3690.
68. Oostenbrink, C., A. Villa, A. E. Mark, and W. F. van Gunsteren. 2004. A biomolecular force field based on the free enthalpy of hydration and solvation: the GROMOS force-field parameter sets 53A5 and 53A6. *J. Comput. Chem.* 25:1656–1676.
69. Stanger, H. E., F. A. Syud, J. F. Espinosa, I. Giriat, T. Muir, et al. 2001. Length-dependent stability and strand length limits in antiparallel L β-sheet secondary structure. *Proc. Natl. Acad. Sci. USA.* 2001 98:12015–20.
70. Daura, X., A. E. Mark, and W. F van Gunsteren. 1998. Parametrization of aliphatic CHn united atoms of GROMOS96 force field. *J. Comput. Chem.* 19:535–547.
71. Berendsen, H., J. P. M. Postman, W. F. van Gunsteren, and J. Hermans. 1981. Interaction models for water in relation to protein hydration. *In* Intermolecular Forces. B. Pullman, editor. D. Reidel Publishing Co., Dordrecht. 331–342.
72. Notman, R., M. Noro, B. O'Malley, and J. Anwar. 2006. Molecular basis for dimethylsulfoxide (DMSO) action on lipid membranes. *J. Am. Chem. Soc.* 128:13982–13983.
73. Roccatano, D., G. Colombo, M. Fioroni, and A. E. Mark. 2002. Mechanism by which 2,2,2-trifluoroethanol/water mixtures stabilize secondary-structure formation in peptides: a molecular dynamics study. *Proc. Natl. Acad. Sci. USA.* 99:12179–12184.
74. Hess, B., H. Bekker, H. J. C. Berendsen, and J. G. E. M. Fraaije. 1997. LINCS: a linear constraint solver form molecular simulations. *J. Comput. Chem.* 18:1463–1472.
75. Sreerama, N., and R. W. Woody. 2000. Estimation of protein secondary structure from circular dichroism spectra: comparison of CONTIN, SELCON, and CDSSTR methods with an expanded reference set. *Anal. Biochem.* 287:252–260.
76. Sreerama, N., and R. W. Woody. 1993. A self-consistent method for the analysis of protein secondary structure from circular dichroism. *Anal. Biochem.* 209:32–44.
77. Soto, F., M. Garcia-Guzman, and W. Stuhmer. 1997. Cloned ligand-gated channels activated by extracellular ATP (P2X receptors). *J. Membr. Biol.* 160:91–100.
78. Yoon, M. J., H. J. Lee, J. H. Kim, and D. K. Kim. 2006. Extracellular ATP induces apoptotic signaling in human monocyte leukemic cells, HL-60 and F-36P. *Arch. Pharm. Res.* 29:1032–1041.
79. Doyle, D. A., C. J. Morais, R. A. Pfuetzner, A. Kuo, J. M. Gulbis, et al. 1998. The structure of the potassium channel: molecular basis of K+ conduction and selectivity. *Science.* 280:69–77.
80. Chang, G., R. H. Spencer, A. T. Lee, M. T. Barclay, and D. C. Rees. 1998. Structure of the MscL homolog from *Mycobacterium tuberculosis*: a gated mechanosensitive ion channel. *Science.* 282:2220–2226.
81. Liao, D. I., G. Kapadia, P. Reddy, M. H. Saier, Jr., J. Reizer, et al. 1991. Structure of the IIA domain of the glucose permease of Bacillus subtilis at 2.2-A resolution. *Biochemistry.* 30:9583–9594.
82. Kelly, S. M., T. J. Jess, and N. C. Price. 2005. How to study proteins by circular dichroism. *Biochim. Biophys. Acta.* 1751:119–139.
83. van der Does, C., J. Swaving, W. van Klompenburg, and A. J. M. Driessen. 2000. Non-bilayer lipids stimulate the activity of the reconstituted bacterial protein translocase. *J. Biol. Chem.* 275:2472–2478.
84. Buck, M. 1998. Trifluoroethanol and collegues: cosolvents come of age. Recent studies with peptides and proteins. *Q. Rev. Biophys.* 31:297–355.
85. Andrushchenko, V. V., H. J. Vogel, and E. J. Prenner. 2006. Solvent-dependent structure of two tryptophan-rich antimicrobial peptides and their analogs studied by FTIR and CD spectroscopy. *Biochim. Biophys. Acta.* 1758:1596–1608.
86. DeCamp, M. F., L. DeFlores, J. M. McCracken, and A. Tokmakoff. 2005. Amide I vibration dynamics of N-methylacetamide in polar solvents: the role of electrostatic interactions. *J. Phys. Chem. B.* 109:11016–11026.
87. Brake, A. J., M. J. Wagenbach, and D. Julius. 1994. New structural motif for ligand-gated ion channels defined by an ionotropic ATP receptor. *Nature.* 371:519–523.
88. Egan, T. M., W. R. Haines, and M. M. Voigt. 1998. A domain contributing to the ion channel of ATP-gated P2X2 receptors identified by the substituted cysteine accessibility method. *J. Neurosci.* 18:2350–2359.
89. Song, L., M. R. Hobaugh, C. Shustak, S. Cheley, H. Bayley, et al. 1996. Structure of staphylococcal α-hemolysin, a heptameric transmembrane pore. *Science.* 274:1859–1866.
90. Hill, K., K. Model, M. T. Ryan, K. Dietmeier, F. Martin, et al. 1998. Tom40 forms the hydrophilic channel of the mitochondrial import pore for preproteins. *Nature.* 395:516–521, [see comment].
91. Duarte, A. M., E. R. de Jong, R. Wechselberger, C. P. van Mierlo, and M. A. Hemminga. 2007. Segment TM7 from the cytoplasmic hemichannel from VO-H+-V-ATPase includes a flexible region that has a potential role in proton translocation. *Biochim. Biophys. Acta.* 1768:2263–2270.
92. van der Spoel, D., and H. J. C. Berendsen. 1997. Molecular dynamics simulations of leu-enkephalin in water and DMSO. *Biophys. J.* 72:2032–2041.
93. Shenderovich, M. D., E. K. Katalin, S. Wilke, N. Collins, and V. J. Hruby. 1997. Solution conformationof potent bicyclic antagonist of oxytocin by nuclear magnetic resonance spectroscopy and molecular dynamics simulations. *J. Am. Chem. Soc.* 119:5833–5846.
94. Bennett, M., R. D'Rozario, M. S. Sansom, and P. L. Yeagle. 2006. Asymmetric stability among the transmembrane helices of lactose permease. *Biochemistry.* 45:8088–8095.
95. Kanyalkar, M., S. Srivastava, A. Saran, and E. Coutinho. 2004. Conformational study of fragments of envelope proteins (gp120: 254–274 and gp41: 519–541) of HIV-1 by NMR and MD simulations. *J. Pept. Sci.* 10:363–380.
96. Lu, H., M. Buck, S. E. Radford, and C. M. Dobson. 1997. Acceleration of the folding of hen lysozyme by trifluoroethanol. *J. Mol. Biol.* 265:112–117.
97. Kumar, Y., S. Muzammil, and S. Tayyab. 2005. Influence of fluoro, chloro and alkyl alcohols on the folding pathway of human serum albumin. *J. Biochem. (Tokyo).* 138:335–341.
98. Chitra, R., and P. E. Smith. 2001. Properties of 2,2,2-trifluoroethanol, chloro and alkyl alcohols on folding pathway of human serum albumin. *J. Chem. Phys.* 114:426–435.
99. Cammers-Goodwin, A., T. J. Allen, S. L. Oslick, K. F. McClure, J. H. Lee, et al. 1996. Mechanism of stabilization of helical conformation of polypeptides by water containing trifluoroethanol. *J. Am. Chem. Soc.* 118:3082–3090.
100. Kentsis, A., and T. R. Sosnick. 1998. Trifluoroethanol promotes helix formation by destabilizing backbone exposure: desolvation rather than native hydrogen bonding defines the kinetic pathway of dimeric coiled coil folding. *Biochemistry.* 37:14613–14622.
101. Van Buuren, A. R., and H. J. Berendsen. 1993. Molecular dynamics simulation of the stability of a 22-residue α-helix in water and 30% trifluoroethanol. *Biopolymers.* 33:1159–1166.
102. Kortemme, T., M. Ramirez-Alvarado, and L. Serrano. 1998. Design of a 20-amino acid, three-stranded β-sheet protein. *Science.* 281: 253–256.
103. Blanco, F. J., and L. Serrano. 1995. Folding of protein G B1 domain studied by the conformational characterization of fragments comprising its secondary structure elements. *Eur. J. Biochem.* 230:634–649.
104. de Leeuw, E., and W. Lu. 2007. Human defensins: turning defense into offense? Infect. Disord. Drug Targets. 7:67–70.